Manuscript accepted for publication in Earth and Planetary Science Letters

Crustal folds alter local stress fields as demonstrated by magma sheet – fold interactions in the Central Andes

Matías Clunes [a], John Browning [a, b, c*], José Cembrano [a, b], Carlos Marquardt [c], Agust Gudmundsson [d]

[a] Department of Structural and Geotechnical Engineering, Pontificia Universidad Católica de Chile, Santiago, Chile

[b] Andean Geothermal Centre of Excellence (CEGA), Universidad de Chile, Santiago, Chile

[c] Department of Mining Engineering, Pontificia Universidad Católica de Chile, Santiago, Chile

[d] Royal Holloway University of London, Department of Earth Sciences, Egham TW20 0EX, United Kingdom

*Corresponding email: jbrowning@ing.puc.cl

Abstract

For magma chambers to form or volcanic eruptions to occur magma must propagate through the crust as dikes, inclined sheets and sills. Most models that investigate magma paths assume the crust to be either homogeneous or horizontally layered, often composed of rocks of contrasting mechanical properties. In regions that have experienced orogenesis, like the Andes, the crust has been deformed over several million years, resulting in rock layers that are commonly folded and steeply dipping. The assumption of homogeneous properties or horizontal layering then does not capture all of the potential magma path-crustal interactions. Here we tackle this problem by determining the effect of a crust made of steeply inclined layers in which sills and inclined sheets are emplaced. We combine field observations from a sill emplaced in the core of an anticlinal fold at El Juncal in the Chilean Central Andes,

including lithologies, sill and fold limbs attitude, length and thickness with a suite of finite element method models to explore the mechanical interactions between inclined layers and magma paths. Our results demonstrate that the properties of the host rock layers as well as the contacts between the layers and the geometry of crustal structures all play an important role in magma propagation and emplacement at shallow levels. Sill propagation and emplacement in heterogeneous and anisotropic crustal segments change the crustal stress field promoting sill arrest, deflection or further propagation. Specifically, sills are more likely to be deflected when encountering shallow dipping layers rather than steeply dipping layers of a fold. Mechanically weak contacts encourage sill deflection due to the related rotation of the stress field and this effect is attenuated when the folded layers are steeper. These processes may change the amount and style of recorded surface deformation, with implications for monitoring of active volcanoes.

Keywords: Crustal folds, Magma emplacement, Sills, Inclined sheets, Central Andes

1. Introduction

The process of magma emplacement and storage in the upper crust is controlled, to a large extent, by the structure of the crust, inherited from tectonic processes, through which the magma propagates (Anderson, 1951; Hutton, 1988; Rubin, 1995; Menand, 2011; Gudmundsson, 2011a, 2020). Contrasts in the mechanical properties between different crustal lithologies can alter the distribution of crustal stresses and hence generate local stress field perturbations, which may become favorable or unfavorable for magma propagation (Hutton, 1988; Gudmundsson, 2011a, 2020). It is the crustal stress field that largely determines if a dike will reach the surface to trigger a volcanic eruption or instead if it becomes arrested in the crust, or locally changes its direction of propagation

to form an inclined sheet or sill (Hutton, 1988; Rubin, 1995; Menand, 2008; Gudmundsson, 2011a).

Dikes, sills and inclined sheets are the frozen remains of fluid-driven extension fractures or hydrofractures (Anderson, 1951; Delaney et al., 1986). Dikes form vertical or sub-vertical geological structures that cut their host rocks discordant to the bedding. Inclined sheets also are form discordant to bedding but dip more shallowly or gently than dikes. Sills are commonly horizontal or sub-horizontal geological structures that form concordant with bedding. All these features propagate as predominantly mode I extension fractures and hence extend parallel to the orientation of the maximum principal compressive stress (in geology, $\sigma_{1,)}$ and open normal to the orientation of the minimum principal compressive stress (in geology, σ_3). The nucleation and extension of a dike, inclined sheet or sill then relies on the fluid pressure, which is normally generated by the gases within magma (Gudmundsson, 2011a, 2020; Geshi et al., 2020).

In order to generate a dike or an inclined sheet the magma must first rupture its host rock. This will happen when the combined internal fluid excess pressure (p_e) and the lithostatic pressure (p_l) at depth exceeds both the tensile strength of the host rock (T_0) and the local minimum principal compressive stress (Jaeger 1956; Gudmundsson, 1986):

$$p_l + p_e \geq \sigma_3 + T_0 \quad (1)$$

The lithostatic pressure (overlying host rock pressure) represents the vertical stress σ_v which can be defined as:

$$\sigma_v = \int_0^z \rho_r(z) g \, dz \quad (2)$$

Where ρ_r is the host rock density as a function of depth (z) and g is acceleration due to gravity.

Tensile strength of rocks at depth have been consistently measured in the range of 0.5 to 9 MPa, with the most common values of 2-4 MPa (Amadei and Stephansson, 1997). The tensile strength provides a constraint on the level of magma pressure required to permit rupture. Once a magma chamber has ruptured, the magma propagates by fracturing the rock ahead and is driven by the internal overpressure (p_o), which depends on both the initial excess pressure (p_e) in the chamber at the time of roof rupture and the magma buoyancy. The overpressure is given by Eq. 3, where ρ_r is the host rock density, ρ_f is the fluid (magma) density, g is acceleration due to gravity, h is the height above the point of rupture and σ_d is the differential stress (σ_1 - σ_3) at the hydrofracture depth (Gudmundsson, 2011a):

$$p_o = p_e + (\rho_r - \rho_f)gh + \sigma_d \quad (3)$$

Here the second term of the right-hand side is the buoyancy term. Dike, sill and inclined sheet emplacement generates crustal deformation. It has been demonstrated through geodetic studies in which it has been documented earthquakes and surface uplift or deflation during magma emplacement (e.g. Sigmundsson et al., 2010). Barnett and Gudmundsson (2014) also shows with FEM models that host rock deformation during sill emplacement depends on sill depth and lateral dimensions. Analogue models that use gelatin as a crustal analogue and water as the magma analogue also demonstrate how the crust can be deformed during magma propagation and emplacement (e.g. Kavanagh et al., 2015).

Most dikes never reach the surface to supply magma to form an eruption and instead become stalled or arrested within the Earth's crust (e.g. Pollard and Johnson, 1973). One

85 way by which this happens is that many dikes change their direction, on their path towards
86 the surface, from vertical to horizontal, and hence to form sills. Is the amalgamation of
87 horizontally propagating magma bodies that can promote the formation of large bodies of
88 magma and can eventually form magma chambers or plutons that grow incrementally
89 through the emplacement of successive sills (Menand, 2011; Annen et al., 2015). Hence,
90 our understanding of both volcanic eruptions and the geophysical signals associated with
91 the emplacement and growth of large crustal intrusive bodies relies on a correct diagnosis
92 of the mechanisms that control the formation and growth of dikes and sills.

93 Magma-filled fractures will propagate if the pressure at the crack tip exceed the host rock
94 strength (Anderson, 1905, 1951). The potential maximum tensile stress (σ_{Max}) at the tip
95 of a sill, modelled as an elliptical cavity, is:

96 $$\sigma_{Max} = p_o \left(\frac{L}{U_I} - 1\right) \quad (4)$$

97 Where p_o is the magmatic overpressure, L is the sill length, and U_I is half aperture or
98 opening of the sill. In practice the tensile stress required to rupture the host rock can be
99 many times lower than the potential maximum tensile stress due to stress concentration
100 effects. However, equation 4 can be used to provide estimates for the range of the
101 parameters discussed. More detailed information on the state of stress at fracture tips,
102 including the effects of the process zone, is provided by the framework of fracture
103 mechanics (Gudmundsson, 2011a). For the present purpose, however, Eq. (4) gives
104 sufficient details.

105 Crustal segments that host volcanoes and igneous intrusions are commonly
106 heterogeneous, that is to say they are built by many different layers of rock which may
107 possess very different mechanical properties. However, the vast majority of mechanical
108 and analogue models that simulate crustal deformation induced by magmatic dynamics

assume a homogeneous and isotropic crustal structure (e.g. Mogi, 1958; Okada and Yamamoto, 1991). In the past decades it has been realized that such an approximation does not accurately represent the crust and hence can introduce significant errors when attempting to discern crustal processes. Instead attempts have been made to consider heterogeneous crustal segments (e.g. Masterlak, 2007; Le Corvec et al., 2013; Souche et al., 2019). However, the vast majority of these models assume vertically stratified and horizontal layers of rocks.

Field observations and mechanical models of sills in compressional tectonic regimes indicate that mechanical layering is a less important factor in controlling sill propagation and emplacement (Walker et al., 2016; Stephens et al., 2017; Walker and Gill, 2020). These authors argue that it is the far-field stress state which controls dike and sill geometry and position, where tectonic shortening or extension and crustal anisotropies (i.e. faults, joints and host rock foliation) plays a predominant role, whereas the bedding is only important in cases when a propagating dike or sill can exploit the interfaces between crustal layers, with differences in material properties. It is important to note that these studies, when mentioned the importance, or lack thereof, of layering also predominately assume horizontally layered crustal segments. However, in active volcanic regions were the continental crust experienced prior deformation, the magma must propagate through mechanically stratified and heterogeneous rocks but the layers forming the crust are often not horizontal. The layers can instead be commonly folded and faulted. Furthermore, subduction or collisional tectonics can produce a highly anisotropic regional stress fields, which further complicate the issue. As such, new models are needed, based on field evidence, to understand the dynamics of magma propagation and crustal storage in deformed regions such as the Andes.

In this work we document mechanical interactions between magma-filled fractures and folded crustal segment to attempt to explain the influence of the geometry of crustal layers on magma propagation and emplacement. We use field data obtained from a rhyodacitic sill emplaced in the core of an anticlinal fold in the central Andes (Figure 2) to build and run 2D models with the Finite-Element Method (FEM) through the software COMSOL Multiphysics. We build model setups with realistic structural settings from field observations (sill and fold layers thickness, length, attitude and host rock stratigraphy) and literature-derived mechanical properties (overpressure and stiffness). The models seek to replicate the observed structures and geometries under certain mechanical conditions during sill emplacement. For this we have developed a series of models varying the stiffness and inclination of the fold layers, mechanical properties of the contact between fold layers and external loading conditions. The studied sill was previous interpreted as a series of syn-tectonic magmatic intrusions due to its geometry, generated according to Piquer et al. (2015) by incremental slip under east-west compression along an active NE-striking dextral fault system with minor NW-NNW-striking faults. The syn-tectonic origin of the sill leads to questions relating to the necessity of active faulting to generate the observed sill geometry and problems relating the magma cooling time and active deformation within the Principal Cordillera.

2. El Juncal sill

In El Juncal, 150 km northeast of Santiago, in the Principal Cordillera of the Chilean Central Andes (Figure 1), a rhyodacitic magma sheet intrudes a series of folded volcanic and volcanoclastic rocks of the Eocene-Miocene Abanico Formation (Piquer et al., 2015; 2019). The Abanico Formation is exposed in the western domain of the Principal Cordillera of the Chilean Central Andes, which is bordered to the east by the Aconcagua folded and faulted bed, a strongly deformed sedimentary rocks from the Mesozoic back-arc basin (Giambiagi

158 et al., 2015; Piquer et al., 2015; 2019). The volcanic and volcanoclastic rocks of the western
159 domain were deposited in an intraarc volcanotectonic basin during the late Eocene to early
160 Miocene (Charrier et al., 2002). During the early Miocene to early Pliocene the basin was
161 inverted due to an E-W directed compression (Giambiagi et al., 2015; Piquer et al., 2019),
162 over which the volcanic Farellones Formation was deposited, covering in discordance the
163 now folded rocks of the Abanico Formation (Charrier et al., 2002; Fock et al., 2006;
164 Giambiagi et al., 2015; Piquer et al., 2019). It is inferred that faults related to this basin
165 controlled the emplacement of magma and hydrothermal fluids (Piquer et al., 2019; 2021)
166 in a region with supergiant porphyry Cu-Mo deposits, such as the Río Blanco-Los Bronces
167 deposit (Crespo et al., 2020). The magma sheet studied in this work has been previously
168 described by Godoy (1998) and then by Piquer et al. (2015) as a sill. This is reasonable
169 since it clearly propagated horizontally. However, an interesting dichotomy in terminology
170 arises from the fact that when the sill meets inclined layers, such as the folded sequence at
171 El Juncal, the emplacement can no longer be concordant to bedding. We expand on this
172 point further in the discussion section. The sill was originally emplaced at a depth of around
173 1-2 km, given the rates of erosion and uplift of the Principal Cordillera from Farías et al.
174 (2008) and Aguilar et al. (2011).
175

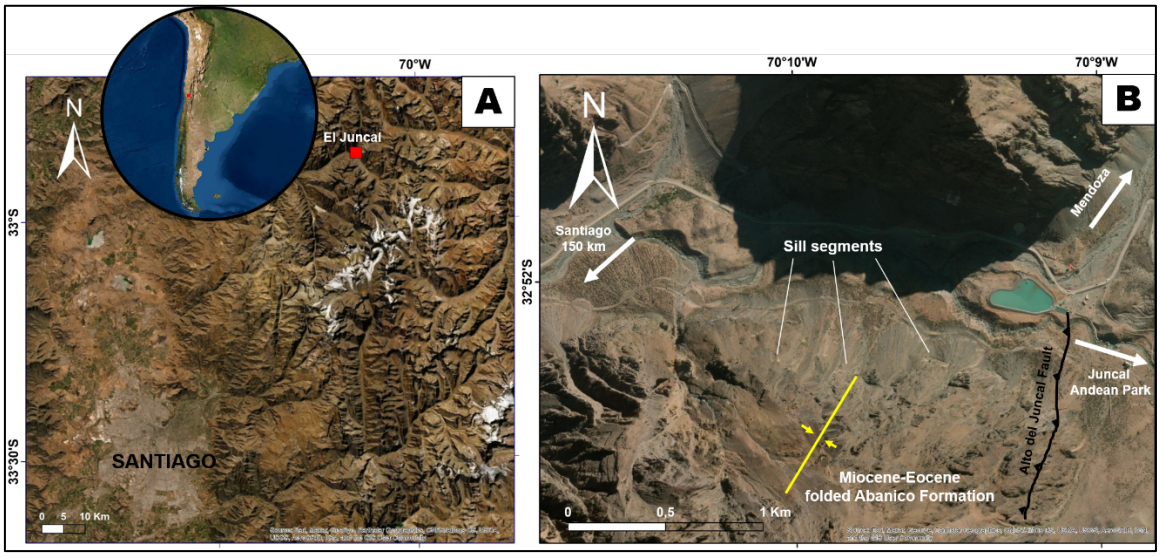

Figure 1. (A) Satellite image of Central Chile. (B) Satellite image and simplified geology of the study area showing the location of sill segments and folds in the Abanico Formation.

176

177 The sill at El Juncal has previously been interpreted as emplaced 'syn-tectonically' within a
178 series of dilational lenses in the core of an East-vergent anticlinal fold related to the Alto del
179 Juncal Fault (Figure 2). Montecinos et al. (2008) obtained a U-Pb zircon age at 11.53±0.19
180 Ma in similar intrusions located to the northeast. The shortening deformation observed in
181 the Principal Cordillera started in the late Oligocene to early Miocene around 25-22 Ma and
182 continues until the present (Charrier et al., 2002; Yáñez and Rivera, 2019; Piquer et al.,
183 2019, 2021). Here we propose an alternative mechanism for the en-echelon segmentation
184 of the sill and consider the interactions between the propagating magma sheet and the
185 crustal layers through which it intruded.

186

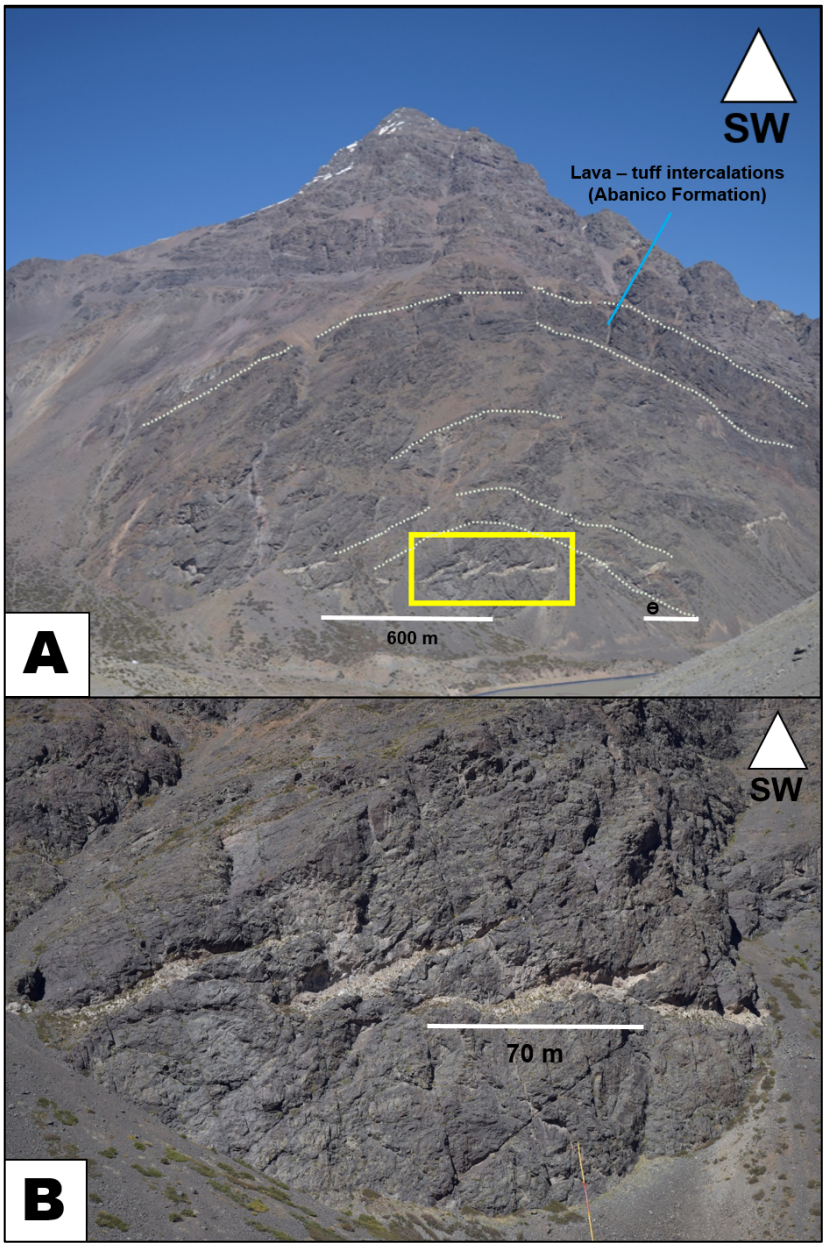

Figure 2. (A) Rhyodacitic segmented magma sheet intruding a heterogeneous and folded crustal segment composed by an alternation of basaltic to andesitic lava flows and tuffs in El Juncal section. The various annotations depict the trace of the folded layers and field measurements. (B) Zoomed in yellow box indicated in A of part of the sill showing the segmented and inclined nature of the tips.

187

188 **3. Mechanisms of sill deflection**

For any magma to reach the surface it must propagate (normally as a magma-filled fracture) through often highly heterogeneous successions. It is generally now well-understood how fractures can become arrested at interfaces between layers in such heterogeneous successions, for example through the processes of 1) stress barriers, 2) elastic mismatch, and 3) Cook-Gordon debonding/delamination (Figure 3). These mechanisms are briefly described below.

1) Stress barriers: as dikes principally nucleate and extend as Mode I extension fractures, they propagate in a direction parallel to the maximum principal stress (σ_1) (Gudmundsson, 2011b). The crustal stresses ahead of a propagating dike can locally rotate because of the way in which different materials, in a heterogeneous succession accommodate stress. If σ_1 rotates from vertical to horizontal this can encourage dike deflection, into a horizontal sill, or it can encourage dike arrest. (Gudmundsson, 1986; Rivalta et al., 2005; Gudmundsson, 2011a; Forbes-Inskip et al., 2020).

2) Elastic mismatch: if there exists a sufficiently large contrast between the stiffness, Young's modulus (E), of two materials in contact this can also promote dike arrest since the level, or magnitude, of tensile stress may not be sufficient to drive the fracture (Gudmundsson, 2011b; Browning and Gudmundsson, 2015). This contrast is called the elastic mismatch and determines, together with material toughness, if a mode I or mixed mode fracture (Rubin, 1995; Hutchinson, 1996) will penetrate the interface between two layers, or instead deflect into any discontinuity between them (He et al., 1994; Hutchinson, 1996; Kavanagh et al., 2006; Gudmundsson, 2011b).

3) Cook-Gordon debonding/delamination (Cook and Gordon, 1967): the stresses induced from the fluid overpressure within a dike may allow the contact (e.g. a pre-existing lithological contact in the host rock) ahead of the dike to delaminate and open. This

generally occurs when the tensile stress ahead of the dike reach about 20% of the tensile strength of the contact (He and Hutchinson, 1989; Hutchinson, 1996; Gudmundsson, 2011b). In the case where the interface between two different rocks experiences debonding or delamination this will encourage either arrest, as the tensile stress can effectively reduce to zero, or a change in the propagation path of a fracture (Hutchinson, 1996; Gudmundsson, 2011b).

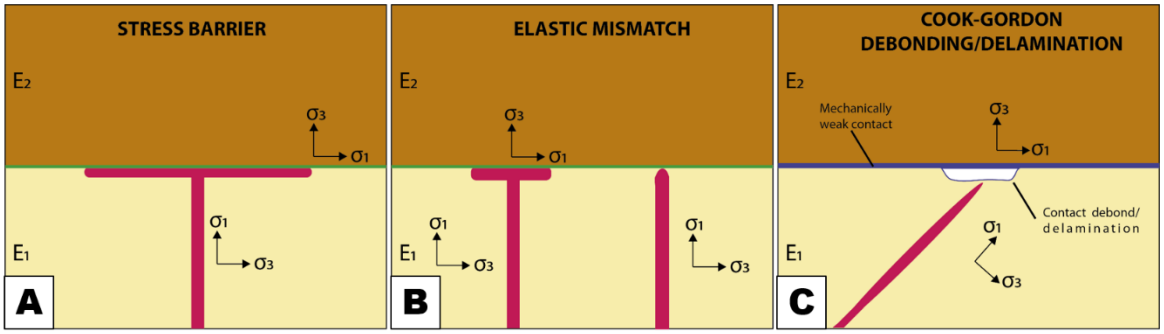

Figure 3. Schematic illustration of primary mechanisms that control fluid-driven fracture arrest, deflection or propagation. (A) Stress barriers. (B) Elastic mismatch. (C) Cook-Gordon debonding and delamination. Modified from Barnet and Gudmundsson (2014) and Drymoni et al. (2020).

The fundamental concepts that derive these models are commonly based on the contacts and layer interfaces being arranged normal to the fracture propagation direction. This situation holds true for heterogeneous crustal segments which are layered sub-horizontally, such as lava piles in shallow dipping volcanic edifices. However, in regions that have experienced intense orogenesis during million years of deformation, like in the Andes, the crustal layers are often intensely deformed and hence fractures meet the contacts and interfaces over a range of different angles. The angle at which a fracture meets a layer or interface has been demonstrated to potentially alter the propagation path (Browning et al., 2015). The stresses in the layers are formed, not just by the regional tectonic forces or the material properties, but also as a function of the geometry of the system. Therefore, an assumption of isotropic material properties and horizontally

232 stratification can lead to highly erroneous results. In the Andean example both
233 assumptions are likely invalid.
234
235 **3. Methods**
236
237 **3.1. Geological succession and material properties**
238
239 We carried out a field campaign at the El Juncal section to record the attitude and thickness
240 of the sill and the units in which the sill was emplaced. The units that the sill cut can be
241 represented by different stiffnesses, that is, by different Young's moduli (E). However, the
242 rocks of the Abanico Formation have been intensely deformed through folding, as can be
243 seen in the compressive structures developed in the Principal Cordillera. This folding makes
244 the rocks stiffer, so originally compliant (soft) and porous rocks like tuffs and many other
245 shallow crustal rocks with E values between 1 and 15 GPa (Becerril et al., 2013), may
246 become more stiffer, i.e., with higher Young's moduli (Gudmundsson, 2011b). In order to
247 model these crustal materials, we used different combinations of layer stiffness in a range
248 between 10 to 40 GPa. This range is slightly higher than that found in recent test on volcanic
249 rocks (Heap et al., 2020) which suggest volcanic rocks will commonly have Young's moduli
250 below 10 GPa, even at depth. However, since we were not able to directly measure the
251 moduli of the rocks, we prefer to use a larger range to encompass more possible
252 combinations of Young's moduli contrast and choose slightly higher values to encompass
253 the effect of compressional strengthening. It could be argued that mechanical
254 measurements are not representative of the rock properties at the time of emplacement
255 since the whole unit has undergone unroofing and has been eroded and weathered. As such
256 we model the various potential range of properties and draw conclusions based on the most
257 realistic values. Based in the Abanico Formation stratigraphy and field observations, we

model the host rock as formed by an intercalation of basaltic lava flows and pyroclastic rocks (Fock et al., 2006). We modelled the contacts between fold layers as either mechanically strong or mechanically weak. Weak contacts were modelled as a 'thin elastic layer', that is, an internal spring with a toughness of 1 MPa/m with an elastic behavior which allows the opening of the contact. Strong contacts were given the same stiffness as the surrounding layers, i.e., in the range 10 to 40 GPa. We gave all the rock units the same Poisson's ratio of 0.25.

3.2 Numerical modelling methods

We use the Finite-Element Method (FEM) software COMSOL Multiphysics to build and run numerical models of 2D cross-sections through the observed folded segment. Using the Structural Mechanics module, in COMSOL we analyze static stress and strains calculated from imposed boundary conditions and solid-mechanical properties in a linear-elastic media. We assign different stiffness values (E) to the layers in a limb of an anticlinal fold based on the host rock geometry and stratigraphy. Also, we change layer inclination (dip) to test how the angle formed between the sill tip and the layers influences the fracture propagation and sill emplacement.

3.3.1 Model setup

We modelled the sill as a singular elliptical cavity with a length of 600 m, a thickness of 15 m and an overpressure (p_o) of 5 MPa. The crust in our models is simplified from that observed in the outcrop and is formed of a layered and folded sequence where each layer has a thickness of 50 m, and they are inclined at either 25° or 50°. These values represent either averages or extremes recorded from the field measurements and hence allow us to

284 examine a wider set of parameters in the models. We consider internal variations in Young's
285 moduli between the layers. We also modelled layers with contrasting Young's moduli, in
286 order to investigate elastic mismatch mechanisms. For this, we considered intercalations of
287 stiff (lava flows) and soft (pyroclastic rocks) layers with Young's moduli of 40 GPa and 10
288 GPa, respectively. For all the models we fixed the lower and horizontal boundaries while the
289 upper boundary is a free surface (Figure 4). We also applied a horizontal compression by
290 applying a load of 5 MPa at the horizontal edges of the model, emulating the regional stress
291 field in a compressive tectonic regime.
292
293 In order to run the models, we generated a triangular mesh with element sizes of between
294 0.235 km (maximum element size) and $1x10^{-3}$ km (minimum element size). The modelled
295 area of interest was built sufficiently far from the model boundaries so not to be affected by
296 edge effects. In all model results we show the magnitude of minimum principal compressive
297 stress (σ_3) as contours showing the location of the highest tensile stress concentration as
298 well as a plot of the trajectories of the maximum principal compressive stress (σ_1), as red
299 ticks.

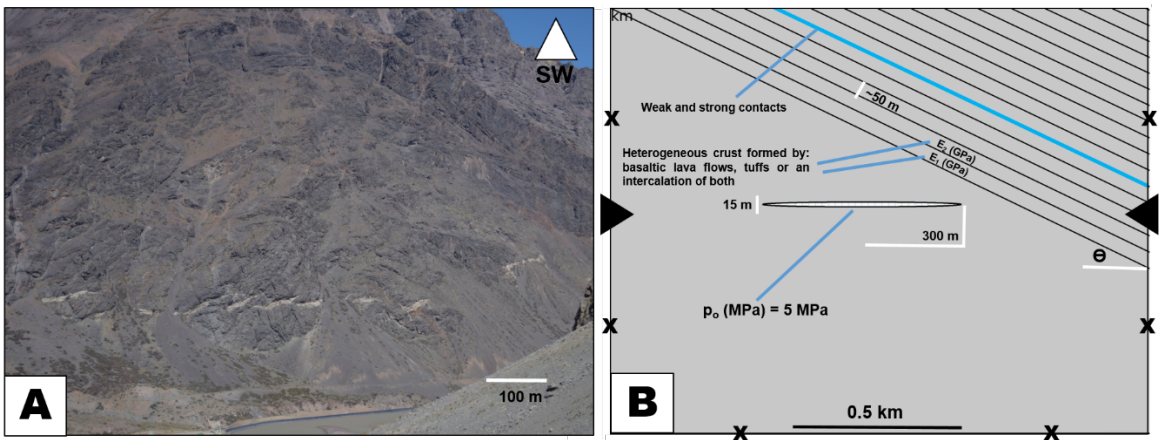

Figure 4. (A) Rhyodacitic sheet segments emplaced in the core of an anticlinal fold (white lines) in the Abanico Formation. (B). Corresponding FEM model setup 2D section example produced in COMSOL Multiphysics, where ϴ represents fold limb inclination.

4. Results

4.1. Field results

The maximum thickness of the studied sill is approximately 15 m thick and it is exposed as a near-horizontal (0-5° dip) magmatic sheet which steepens to 20° and 30° to the SW at the tips of a series of en-echelon segments. The sill strikes approximately WNW-ESE (Figure 4) and is mostly sub-horizontal along both its strike and dip lengths. The exposed section of the sill is around 600 m in length and each segment is between 50 m to 70 m in length. The sill composition is rhyodacitic with porphyritic texture composed of plagioclase phenocrysts in a groundmass of fine feldspar and quartz (Montecinos et al., 2008; Piquer et al., 2015). The sill is emplaced in the core of a NE-trending open, predominantly symmetrical, anticlinal fold with limbs that dip by a maximum of 25° to the NW and SE. The fold is formed in intercalations of andesitic to basaltic lava flows and tuffs of the Miocene-Eocene Abanico Formation, in beds of approximately 50 m in thickness. We found no evidence of shear-related displacement of the units at the sill tips of the en-echelon segments.

4.2. Numerical modelling results

4.2.1. Fold limbs dipping away from the sill

In Figure 5 we show the modelled interaction between the horizontal cavity (the sill) with an internal pressure of 5 MPa near a series of layers dipping or inclined at 25° away from the sill. In part A (Figure 5) the layers all have the same material properties, namely, a Young's modulus of 10 GPa and the contacts between the layers are mechanically strong, i.e. they

have the same stiffness as the surrounding rocks. Whereas in Part B (Figure 5) the layers again all have the same material properties (E = 10 GPa) but the contacts in between the layers are mechanically weak. In Figure 5a we see that the tensile stress concentrations occur at the lateral ends of the sill, exactly as expected. We also see that the orientation of σ_1, shown as red lines in the model figures continue approximately horizontally away from the sill margins. This indicates that the dipping layers have little to no influence on the propagation path of the sill and hence it would continue propagating horizontally under these circumstances. However, in Figure 5b we see that the concentration of tensile stresses is quite different as there is a large concentration of stress at the contact between the first layer and the host rock directly above the right side of the sill. We also see stress concentrations in two other layers further away from the sill. These concentrations indicate that the contacts may debond/delaminate and open which will affect the propagation path of the sill. The orientation of σ_1 in this case changes locally from horizontal to vertical at the contact between the sill and the inclined layers at 25°. These rotations may promote either the arrest or the deflection of the sill as σ_1 rotates by 90° in some of the layer contacts.

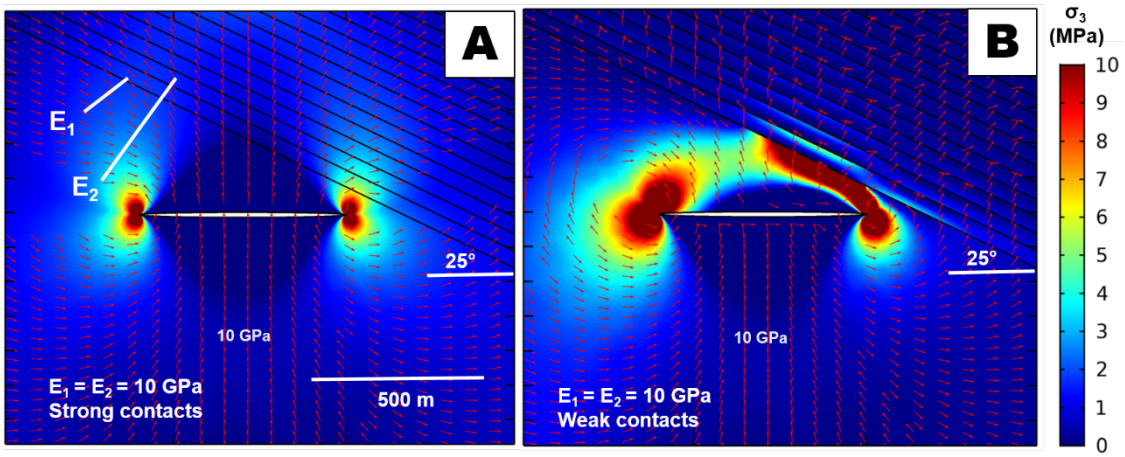

Figure 5. FEM (finite element method) models of stresses around a sill near a homogeneous (E_1=E_2) crustal segment with layers dipping at 25° away from the sill. The red arrows show the trajectories of the

maximum compressive principal stress, σ_1, and color contours represent the minimum principal compressive (maximum tensile) principal stress, σ_3. (A) The contacts between the layers are modelled as mechanically strong. (B) The contacts between the layers are modelled as mechanically weak, and therefore with tendency to open up.

342

343 In Figure 6 the geometry of the model is the same as previously but now the layers are
344 heterogeneous, that is to say that they have different Young's moduli. In Figure 6a and 6b
345 the layer closest to the sill is softer (10 GPa) than the succeeding layer (40 GPa). Whereas
346 in Figure 6c and 6d, the layer closest to the sill is stiffer (40 GPa) than the succeeding layer
347 (10 GPa). We again consider two different types of contact properties between the layers.
348 In Figure 6a and 6c, the contacts were modelled as strong contacts with the same Young's
349 moduli of the respective layers, meanwhile in Figure 6b and 6d, the contacts were modelled
350 as mechanically weak, with a stiffness of 1 MPa/m. We observe from Figure 6a that if the
351 sill is near to a series of softer layers but with a mechanically strong contact, the tensile
352 stress concentrations are located at the sill tip in the host rock with very little stress
353 concentration in the soft layer but with high tensile stresses in the succeeding stiff layer. The
354 trajectories of the maximum principal stress (σ_1) in this case continue almost horizontally
355 away from the sill tips. This indicates that the sill would continue a horizontal propagation
356 path through the sill. In Figure 6b the properties of the layers are the same but the contacts
357 between the layers are mechanically weak. Under these conditions we observe large tensile
358 stress concentrations at the sill tip and directly above the sill in the host rock but virtually
359 none of that stress is concentrated within the dipping layers. This indicates that the first
360 contact between the host rock and the dipping layers may debond (delaminate) under the
361 high tensile stress. The orientations of σ_1 rotate by 90° at the contacts between the layers.
362 Both the propensity for debonding and the strong stress rotations indicate the sill would likely
363 become arrested at the contact with the dipping layers. In Figure 6c we alternate the stiffness

of the layers and we observe that the tensile stress concentrations again occur only in the stiff units but in contrast to previously all the stiff layers in the segment experience and elevated stress level. The orientation of σ_1 is again near horizontal throughout. In Figure 6d several stiff layers concentrate tensile stress directly below the weak contacts, this is especially pronounced between the first and second layers within the dipping units. As we observed in Figure 6b, in Figure 6d, the orientations of σ_1 also change from near vertical to rotate almost 90° and follow the dip of the layers.

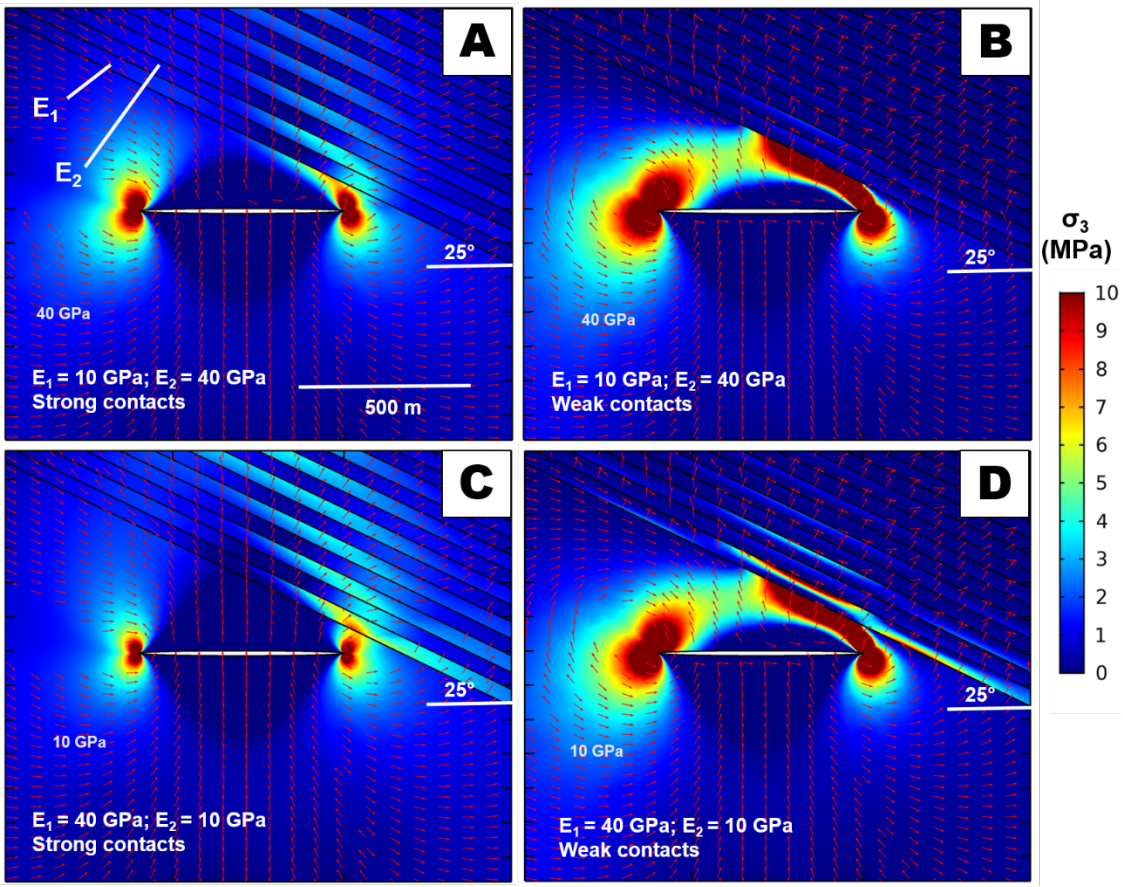

Figure 6. FEM (finite element method) models of stresses around a sill near a heterogeneous (E_1>E_2) crustal segment with layers dipping at 25° away from the sill. The red arrows show the trajectories of the maximum compressive principal stress, σ_1, and color contours represent the minimum principal

compressive (maximum tensile) principal stress, σ_3. (A) The contacts between the layers are modelled as mechanically strong. (B) The contacts between the layers are modelled as mechanically weak.

372

373 The model setups shown in Figures 7 and 8 have the same mechanical conditions as
374 previously shown but the geometry of the model has been changed. Specifically, we change
375 the dip of the layers that constitute the fold from 25° in the previous models (Figures 5 to 6)
376 to 50° (Figures 7 and 8). The result from the model in which the layers have the same
377 Young's modulus throughout the fold limbs (Figure 7a) are almost the same as the previous
378 results shown (Figure 5). This suggests that if the layers in a folded segment are of similar
379 properties, the inclination of the fold has little effect on the propagation path of a magma
380 sheet. However, in Figure 7b, where there are weak contacts between the layers, the results
381 are quite different from the previous models. Namely, whilst we still observe high levels of
382 tensile stress concentration at the margins of the sill and specifically above the right margin,
383 we do not observe rotation of the principal stresses in the layers of the fold limb. This
384 difference needs to be explained and we discuss this point further in the discussion section.

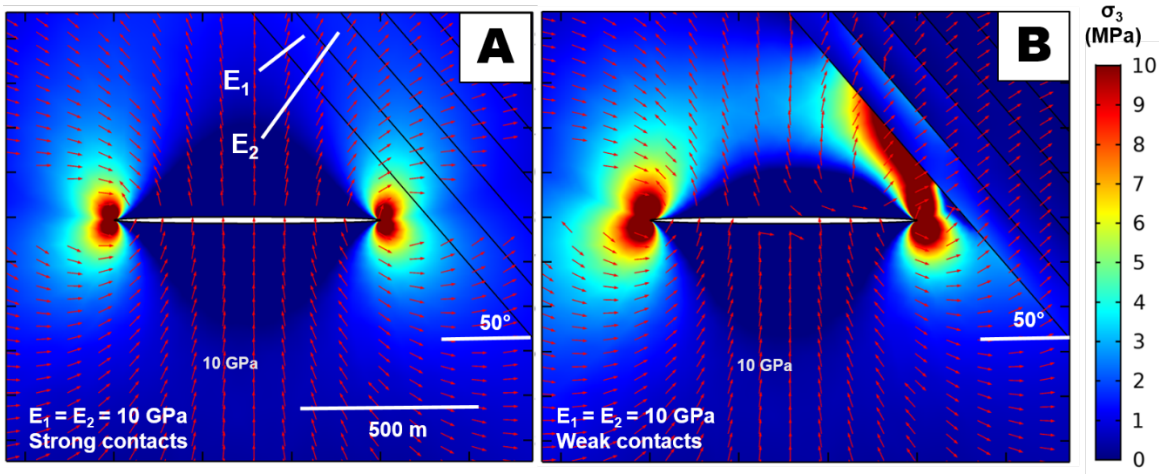

Figure 7. FEM (finite element method) models of stresses around a sill near a homogeneous (E_1=E_2) crustal segment with layers dipping at 50° away from the sill. The red arrows show the trajectories of the maximum compressive principal stress, σ_1, and color contours represent the minimum principal compressive (maximum

tensile) principal stress, σ_3. (A) The contacts between the layers are modelled as mechanically strong. (B) The contacts between the layers are modelled as mechanically weak.

385

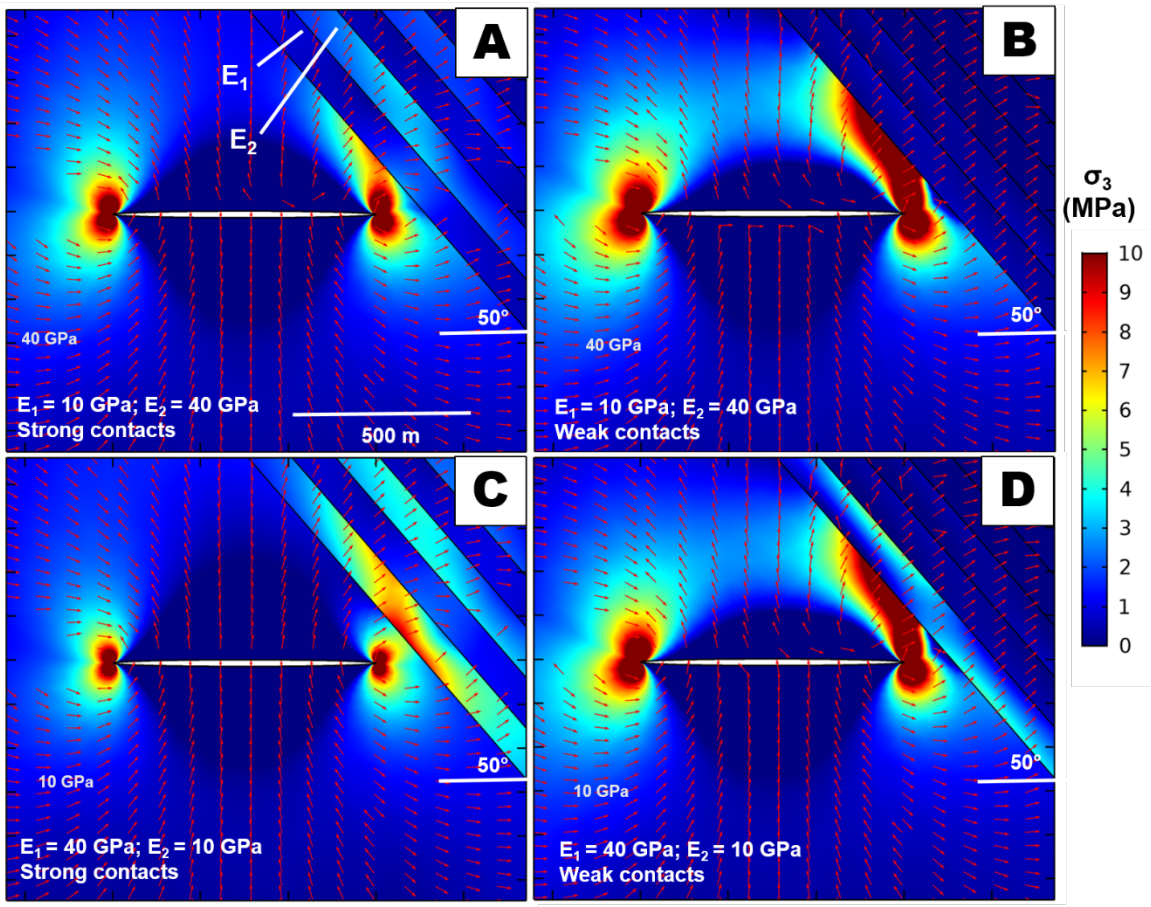

Figure 8. FEM (finite element method) models of stresses around a sill near a heterogeneous (E_1>E_2) crustal segment with layers dipping at 50° away from the sill. The red arrows show the trajectories of the maximum compressive principal stress, σ_1, and color contours represent the minimum principal compressive (maximum tensile) principal stress, σ_3. (A) The contacts between the layers are modelled as mechanically strong. (B) The contacts between the layers are modelled as mechanically weak.

386 **4.2.2. Fold limbs dipping towards the sill**

387

388 We modified the models shown in section 4.2.1 by changing the geometry of the dipping
389 layers such that they dip towards the sill rather than away from it. In the field case the

previous models represented the NW limb of the El Juncal fold, whereas the new models in this section represent the SE limb of the fold. The results are similar throughout the models and so we present the data as Supporting Information. The most striking difference is that the tensile stress concentrations in stiff layers now occur below rather than above the sill tip. This indicates that the debonding/delamination mechanism is less likely a cause of the segmented sill arrangement observed in the field. This holds because the inflection would dip in the opposite direction to that observed. However, the variable stresses in the layers can still promote stress field rotations that encourage the sill to deflect and become an inclined sheet along the dipping layers.

5. Discussion

5.1. Processes that influence the geometry of sills near to crustal folds

We observe from the numerical models that the sill geometry and segmentation in El Juncal depends on the properties and geometry of the fold through which the sill cuts. Specifically, it is the angle at which the layers dip as well as the difference in material properties of the layers and the properties of the contacts between the layers which generate the observed sill geometry. The effect of these geometrical and physical properties combine to locally alter the stress field ahead of the propagating sill and, in the case of El Juncal, this has led to a temporary change in the orientation of the sill from sub-horizontal to incline. Our data is limited to one well-exposed outcrop but the mechanical mechanisms described demonstrate generality and so can be applied to volcanic complexes overlying folded crustal segments. As far as we are aware there have been no attempts to document the interaction of hundreds of meters to kilometer scale folds with magma emplacement. This may be partly because of the lack of such exposures elsewhere. As such we now consider the potential consequences

of processes related to magma sheet and fold interactions in the context of Andean crustal segments hosting active volcanoes.

In the northern part of the southern volcanic zone of the Andes (33°S-37°S), the volcanic arc is built upon a basement formed by heterogeneous and heavily folded rock units as well as numerous crustal faults. As a result of the crustal deformation there are many cases in this zone where the basement rocks are distinctly non-horizontal. As such the dikes, sills and inclined sheets that cut these crustal regions must intersect the layers at different angles. We have demonstrated in the numerical models that the dip of the layers, and hence the angle at which a dike, sill or inclined sheet meets the layers, is important in controlling the distribution of crustal stresses. We find that if the layers are more steeply dipping there is less propensity to arrest a horizontally propagating sill (Figure 9). To understand the reason for this we must consider the compressional effect that the sill has on the overlying and underlying rock layers when it is emplaced in the crust. When a sill is emplaced in a heterogeneous mechanically stratified crustal segment where all the layers are horizontal, the sill will compress (apply a normal force to) the layers above and below. The amount of stress and deformation in those layers is then directly related to their respective Young's moduli and so some layers will accommodate more stress than others. In the case where the layers are shallowly dipping the process is similar. However, when the same horizontal sill is emplaced in a heterogeneous segment comprised of steeply dipping layers with weak contacts between the layers, the compressional effect is much less pronounced. In addition, the contacts between layers may be weakened which can promote debonding/delamination between the layers, allowing the sill to for a time become an inclined sheet (Figure 9). The geometry or orientation of the layers (i.e. whether they dip towards or away from the sill) can also influence magma paths but the mechanism that controls the deflection can be quite different.

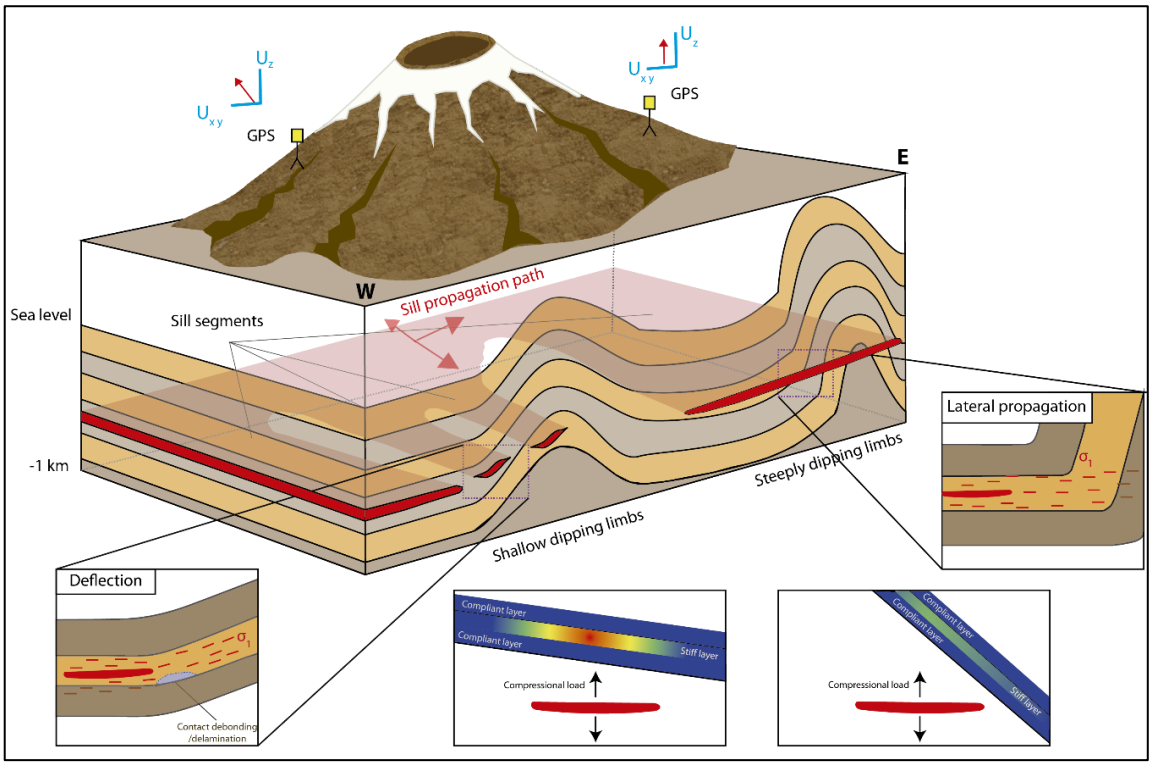

Figure 9: Schematic diagram demonstrating potential sill propagation pathways and associated mechanisms in a crustal segment hosting a central volcano overlying a variably folded sequence of rocks. To the west the sill encounters an anticlinal fold with shallow dipping limbs. The pressure of the sill exerts a compressional load on the overlying rock units and rotates the orientation of σ_1 from horizontal to inclined. Stress rotation can become enhanced if the contacts between the rock layers are weak. During a period of unrest, the surface deformation signal from such an emplacement event would be a composite of both the vertical sill opening and the segmented inclined sheet opening. To the East of the crustal segment the sill encounters an anticlinal fold with steep limbs. The compressional load of the sill can now not stress the overlying rock units as they are unfavorably oriented. The consequence is that the sill continues its horizontal propagation path. During a period of unrest, the surface deformation signal would be dominated by vertical opening of the sill.

5.2. Does the observed sill arrangement require faulting to form?

The uncharacteristic arrangement of the studied sill at El Juncal has previously been interpreted as forming syn-tectonically within a set of dilational lenses (Godoy, 1998; Piquer

et al., 2015). These dilational lenses are formed by differential motion on fault blocks generating local tension. This interpretation requires a complex set of shear related structures and such structures have important implications for the location and development of ore forming minerals (Piquer et al., 2015). The interpretation then also requires that as the sill propagated it exploited these shear structures to form the en-echelon and inclined structures observed at the segment's sill tips. However, this cannot explain why the sill did not continue to follow the shear zones to become an inclined sheet, as could be expected (Gudmundsson, 2002). Also, the notion of syn-tectonic emplacement is somewhat unhelpful because it requires that all of the shear zones in question become displaced in order to form the structures observed which is a remarkable hypothesis that is not supported by any geophysical measurements from any active magma emplacement anywhere in the world, as far as we are aware. The term 'syn-tectonic' may also imply that the sill and fold were deforming at the same time but this generates a significant temporal problem since deformation related to the fold formation occurs over thousands or millions of years whereas the dike emplacement and subsequent solidification takes place over the order of months to years (Carslaw and Jaeger, 1959; Gudmundsson, 2020).

We have demonstrated that changes in the orientation of the sill can relate to the properties of the rocks through which the sheet is emplaced, and hence changes in the local crustal stress field, rather than requiring a 'syn-tectonic' shear related deformation. We found that substantial changes in orientation can be produced when there are weak contacts between layers. Such weak contacts may be produced by the presence of crustal faults, for example. We hence partly support the view of Godoy (1998) and Piquer et al. (2015) in that the sill may inflect because of the presence of shear zones but we cannot support the notion that there were dilational lenses formed within the shear zones as this is not supported by mechanical models of sill and dike propagation (Gudmundsson, 2020).

5.3. Implications for shallow intrusion nomenclature

In this manuscript we consider a magma body that has propagated several kilometers sub-horizontally. It is then reasonable to call that magma body a sill. However, the sill is not always concordant with bedding, as is required in the nomenclature for a sill (Emerman and Marret, 1990). In fact, when the sill meets a folded segment, or crustal discontinuity, it can cut the layers discordantly. Hence the El Juncal sill, which we have described, in nomenclature, would be considered an inclined sheet since it is discordant with many of the folded layers. What we have shown in our numerical models is that the 'inclined sheet' then attempts to become a 'sill' when it meets the folded layers by partly following the attitude of the layers. This is somewhat of a semantic point but it is important to clarify. The inflections of the intrusion segments observed at El Juncal occur over scales of a few meters and so there is a clear difference with the geometry of much larger, tens to hundreds of meters, scale saucer-shaped sills (Magee et al., 2013).

5.4 Implications for ground surface deformation

Our results have implications for the style of ground surface deformation induced by sill emplacement in Andean crustal segments. A significant proportion of the active volcanoes in the Andes are built, at least partially, on folded crustal sequences, for example, the Pleistocene-Holocene volcanoes located between 23°S-24°S in northern Chile, and those active volcanoes located between 33°S-37°S (Cembrano and Lara, 2009). The mechanical interactions described in this work can also be applied to other tectonic settings where there is active volcanism developed upon a deformed continental crust. For example, in settings where volcanoes are built upon older fold and thrust belts, the emplaced magma must first

propagate through these folded rock units even if the active volcanism occurs under continental rifting or post-collisional extensional stress environments. So, a problem then becomes: how do we correctly interpret the ground surface deformation signal if a sill is emplaced within the crust beneath one of these active volcanic complexes? One could envisage the crustal deformation from a horizontally emplaced sill, or and inclined sheet, as is commonly done using the Okada dislocation model (Okada, 1985). Inclined layers can influence magma propagation and emplacement and so the geometry, as well as the heterogeneity (Masterlak, 2007) of crustal units should be considered in models of volcano deformation. The style and amount of ground deformation can provide useful information about the mechanism of impending volcanic eruptions (Mogi, 1958; Masterlak, 2007; Geshi et al., 2020). We have demonstrated that a horizontally propagating sill can for a time become inclined due to interactions with crustal folds, changing the crustal stress field. These interactions and changes in orientation are localized, as has been recognized elsewhere (Stephens et al., 2017), but the implications in terms of interpreting crustal deformation signals can become complex and important (Figure 9). The question then arises what would be the deformation signal from such a complex emplacement event? We recommend further work on this topic.

6. Conclusions

When taken together our results demonstrate the importance of having a complete understanding of the stratigraphy and geometry of crustal segments. This is especially important in active orogenic regions, either in subduction zones like the Andes and collisional or extensional tectonic settings (e.g. in the post-collisional volcanos located in the northern part of the Arabia-Eurasia collision zone and in the continental rift of eastern Africa)

where tectonic forces have intensely compressed and deformed the continental crust and so the rock units are often not horizontal. The main conclusions of our study are as follows:

1) Sill emplacement through inclined layers changes the crustal stress field promoting sill arrest, deflection or propagation. We suggest that a crust hosting shallow dipping layers will more easily encourage sill deflection, whereas a crust hosting steeply dipping layers promotes continued lateral sill propagation.

2) The mechanical properties of the contacts between layers strongly controls magma propagation and emplacement. Mechanically weak contacts encourage sill deflection due to stress field rotation. The result of this process can be observed in sill geometries at El Juncal. This effect is attenuated when the layers are inclined at higher angles.

3) Sill propagation and emplacement through folded crustal segments may generate surface deformation that will become a composite of both vertical deformations, from the opening of a horizontal sill, and combined vertical-horizontal deformation formed from inclined segments of the predominantly vertically opening sill. Associated deformation signals can be measured at actively monitored volcanoes and crustal layering and folding should be considered when modelling these deformation signals.

Acknowledgements

We thank the editor Alex Webb, as well Alessandro Tibaldi and an anonymous reviewer for comments and suggestions that helped improve the manuscript. This research was funded

551 by the National Agency for Research and Development (ANID), through the programs ANID-
552 FONDECYT, Project 11190143; and ANID-FONDAP, Project 15090013. Matías Clunes
553 acknowledges support from ANID Scholarship Program, Beca de Doctorado Nacional
554 21202065. Further data is given in a supporting information file and the full dataset can be
555 obtained from JB at jbrowning@ing.puc.cl.
556
557 **References**
558
559 Amadei, B., Stephansson, O., 1997. Rock stress and its measurement. (Chapman Hall,
560 New York).
561
562 Anderson, E. M., 1905. The dynamics of faulting. Transactions of the Edinburgh Geological
563 Society, 8(3), 387-402.
564
565 Anderson, E.M., 1951. Dynamics of faulting and dyke Formation. 2nd edn. Olivier and Boyd,
566 Edinburgh.
567
568 Annen, C., Blundy, J. D., Leuthold, J., Sparks, R. S. J., 2015. Construction and evolution of
569 igneous bodies: Towards an integrated perspective of crustal magmatism. Lithos, 230, 206-
570 221.
571 Barnett, Z., Gudmundsson, A., 2014. Numerical modelling of dikes deflected into sills to form
572 a magma chamber. Journal of Volcanology and Geothermal Research, 281, 1-11.
573
574 Becerril, L., Galindo, I., Gudmundsson, A., Morales, J.M., 2013. Depth of origin of magma
575 in eruptions. Sci. Rep. 3, 2762. https://doi.org/10.1038/srep02762.

Browning, J., Drymoni, K., Gudmundsson, A., 2015. Forecasting magma-chamber rupture at Santorini volcano, Greece. Scientific reports, 5, p.15785

Browning, J., Gudmundsson, A., 2015. Caldera faults capture and deflect inclined sheets: an alternative mechanism of ring dike formation. Bulletin of Volcanology, 77(1), 4.

Carslaw, H.S., Jaeger, J.C., 1959. Conduction of heat in solids. 2nd ed. Clarendon Press, Oxford, UK.

Charrier, R., Baeza, O., Elgueta, S., Flynn, J.J., Gans, P., Kay, S.M., Muñoz, N., Wyss, A.R., Zurita, E., 2002. Evidence for Cenozoic extensional basin development and tectonic inversion south of the flat-slab segment, southern Central Andes, Chile (33º-36ºS.L.). Journal of South American Earth Sciences 15: 117-139.

Cembrano, J., Lara, L., 2009. The link between volcanism and tectonics in the southern volcanic zone of the Chilean Andes: a review. Tectonophysics, 471(1-2), 96-113.

Cook, J., Gordon, J.E., 1964. A mechanism for the control of crack propagation in all-brittle systems. Proceedings of the Royal Society 282, 1364–5021.

Crespo, J., Reich, M., Barra, F., Verdugo, J. J., Martínez, C., Leisen, M., Romero, R., Morata, D., Marquardt, C., 2020. Occurrence and Distribution of Silver in the World-Class Río Blanco Porphyry Cu-Mo Deposit, Central Chile. Economic Geology, 115(8), 1619-1644.

601 Delaney, P. T., Pollard, D. D., Ziony, J. I., McKee, E. H., 1986. Field relations between dikes
602 and joints: emplacement processes and paleostress analysis. Journal of Geophysical
603 Research: Solid Earth, 91(B5), 4920-4938.
604 Drymoni, K., Browning, J., Gudmundsson, A., 2020. Dike-arrest scenarios in extensional
605 regimes: Insights from field observations and numerical models, Santorini, Greece. Journal
606 of Volcanology and Geothermal Research, 106854.
607
608 Emerman, S. H., Marrett, R., 1990. Why dikes?. Geology, 18(3), 231-233.
609
610 Fock, A., Charrier, R., Farías, M., Muñoz, M., 2006. Fallas de vergencia oeste en la
611 Cordillera Principal de Chile Central: Inversión de la cuenca de Abanico (33-34 S). *Revista*
612 *de la Asociación Geológica Argentina, Publicación Especial*, *6*, 48-55.
613
614 Forbes-Inskip, N.D., Browning, J., Meredith, P.G., Gudmundsson, A., 2020. Conditions for
615 fracture arrest in layered rock sequences. Results in Geophysical Sciences, 1, p.100001.
616
617 Geshi, N., Browning, J., Kusumoto, S., 2020. Magmatic overpressures, volatile exsolution
618 and potential explosivity of fissure eruptions inferred via dike aspect ratios. Scientific
619 Reports, 10(1), pp.1-9.
620
621 Giambiagi, L., Tassara, A., Mescua, J., Tunik, M., Alvarez, P. P., Godoy, E., Hoke, G., Pinto,
622 L., Spagnotto, S., Porras, H., Tapia, F., Jara, P., Bechis, F., García, V., Suriano, J., Maris
623 Moreiras, S., Pagano, S. D., 2015. Evolution of shallow and deep structures along the
624 Maipo–Tunuyán transect (33° 40′ S): from the Pacific coast to the Andean foreland.
625 Geological Society, London, Special Publications, 399(1), 63-82.
626

627 Godoy, E., 1998. Intrusivos sintectónicos entre los ríos Aconcagua y Cachapoal, Andes de
628 Chile Central: Sociedad Geologica de Chile, Congreso Latinoamericano de Geología, 10th,
629 Concepción, Chile, 1998, Proceedings, v. 2, p. 149–154.
630
631 Gudmundsson, A., 1986. Mechanical aspects of postglacial volcanism and tectonics of the
632 Reykjanes Peninsula, southwest Iceland. Journal of Geophysical Research: Solid Earth,
633 91(B12), 12711-12721.
634
635 Gudmundsson, A., 2011a. Rock fractures in geological processes. Cambridge University
636 Press. 578.
637
638 Gudmundsson, A., 2011b. Deflection of dikes into sills at discontinuities and magma-
639 chamber formation. Tectonophysics, 500(1-4), 50-64.
640
641 Gudmundsson, A., 2020. Volcanotectonics: Understanding the Structure, Deformation and
642 Dynamics of Volcanoes. Cambridge University Press.
643
644 He, M. Y., Hutchinson, J. W., 1989. Kinking of a crack out of an interface.
645
646 Heap, M.J., Villeneuve, M., Albino, F., Farquharson, J.I., Brothelande, E., Amelung, F., Got,
647 J.L., Baud, P., 2020. Towards more realistic values of elastic moduli for volcano modelling.
648 Journal of Volcanology and Geothermal Research, 390, p.106684.
649
650 Hutchinson, J. W., 1996. Stresses and failure modes in thin films and multilayers. Notes for
651 a Dcamm Course. Technical University of Denmark, Lyngby, 1.
652

653 Hutton, D. H., 1988. Granite emplacement mechanisms and tectonic controls: inferences
654 from deformation studies. Earth and Environmental Science Transactions of the Royal
655 Society of Edinburgh, 79(2-3), 245-255.
656
657 Jaeger, J. C., 1956. Elasticity, Fracture and Flow, 152. Methuen, New York.
658
659 Kavanagh, J. L., Menand, T., Sparks, R. S. J., 2006. An experimental investigation of sill
660 formation and propagation in layered elastic media. Earth and Planetary Science Letters,
661 245(3-4), 799-813.
662
663 Kavanagh, J. L., Boutelier, D., Cruden, A. R., 2015. The mechanics of sill inception,
664 propagation and growth: Experimental evidence for rapid reduction in magmatic
665 overpressure. *Earth and Planetary Science Letters*, *421*, 117-128.
666
667 Le Corvec, N., Menand, T., Lindsay, J., 2013. Interaction of ascending magma with pre-
668 existing crustal fractures in monogenetic basaltic volcanism: an experimental approach. J.
669 Geophys. Res. 118 (3), 968–984.
670
671 Magee, C., Hunt-Stewart, E., Jackson, C. A. L., 2013. Volcano growth mechanisms and the
672 role of sub-volcanic intrusions: Insights from 2D seismic reflection data. Earth and Planetary
673 Science Letters, 373, 41-53.
674
675 Masterlark, T., 2007. Magma intrusion and deformation predictions: Sensitivities to the Mogi
676 assumptions. Journal of Geophysical Research: Solid Earth, 112(B6).
677

678 Menand, T., 2011. Physical controls and depth of emplacement of igneous bodies: A review.
679 Tectonophysics, 500(1-4), 11-19.
680
681 Mogi, K., 1958. Relations between the eruptions of various volcanoes and the deformations
682 of the ground surface around them, Bull. Earthquake Res. Inst. Univ. Tokyo, 36, 99– 134.
683 Montecinos, P., Schärer, U., Vergara, M., Aguirre, L., 2008. Lithospheric origin of
684 Oligocene–Miocene magmatism in Central Chile: U–Pb ages and Sr–Pb–Hf isotope
685 composition of minerals. Journal of Petrology, 49(3), 555-580.
686
687 Okada, Y., Yamamoto, E., 1991. Dyke intrusion model for the 1989 seismovolcanic activity
688 off Ito, central Japan. Journal of Geophysical Research: Solid Earth, 96(B6), 10361-10376.
689
690 Piquer, J., Skármeta, J., Cooke, D. R., 2015. Structural Evolution of the Rio Blanco-Los
691 Bronces District, Andes of Central Chile: Controls on Stratigraphy, Magmatism, and
692 Mineralization. Economic Geology, 110(8), 1995-2023.
693
694 Piquer, J., Yáñez, G., Rivera, O., Cooke, D. R., 2019. Long-lived crustal damage zones
695 associated with fault intersections in the high Andes of Central Chile. Andean Geology,
696 46(2), 223-239.
697
698 Piquer, J., Sánchez-Alfaro, P., Pérez-Flores, P., 2021. A new model for the optimal structural
699 context for giant porphyry copper deposit formation. Geology.
700

701 Pollard, D.D., Johnson, A.M., 1973. Mechanics of growth of some laccolithic intrusions in
702 the Henry mountains, Utah, II: bending and failure of overburden layers and sill formation.
703 Tectonophysics 18 (3–4), 311–354.
704
705 Rivalta, E., Böttinger, M., Dahm, T., 2005. Buoyancy-driven fracture ascent: Experiments in
706 layered gelatine. Journal of Volcanology and Geothermal Research, 144(1-4), 273-285.
707
708 Rubin, A. M., 1995. Propagation of magma-filled cracks. Annual Review of Earth and
709 Planetary Sciences, 23(1), 287-336.
710
711 Sigmundsson, F., Hreinsdottir, S., Hooper, A., Árnadóttir, T., Pedersen, R., Roberts, M. J.,
712 Óskarsson, N., Auriac, A., Decriem, J., Einarsson, P., Geirsson, H., Hensch, M., Ófeigsson,
713 B. G., Sturkell, E., Sveinbjörnsson, H., Feigl, K. L., 2010. Intrusion triggering of the 2010
714 Eyjafjallajökull explosive eruption, Nature, 468, 426–430, doi:10.1038/nature09558, 2010.
715
716 Stephens, T.L., Walker, R.J., Healy, D., Bubeck, A., England, R.W. McCaffrey, K.J., 2017.
717 Igneous sills record far-field and near-field stress interactions during volcano construction:
718 Isle of Mull, Scotland. *Earth and Planetary Science Letters*, *478*, pp.159-174.
719
720 Walker, R. J., 2016. Controls on transgressive sill growth. Geology, 44(2), 99-102.
721
722 Walker, R.J., Gill, S.P.A., 2020. Tectonic stress controls saucer-shaped sill geometry and
723 emplacement mechanism. *Geology*.
724

725 Yáñez, G., Rivera, O., 2019. Crustal dense blocks in the fore-arc and arc region of Chilean
726 ranges and their role in the magma ascent and composition: Breaking paradigms in the
727 Andean metallogeny. Journal of South American Earth Sciences, 93, 51-66.

Declaration of Interest Statement

The authors declare no conflict of interest with respect to the preparation and publication of themanuscript '*Crustal folds alter local stress fields as demonstrated by magma sheet – fold interactions in the Central Andes*'

Credit Author Statement

Credit author statement

Matias Clunes, John Browning Conceptualization, Methodology, Writing - Original draft preparation, reviewing, editing, **Jose Cembrano, Carlos Marquardt, Agust Gudmundsson** Writing-reviewing, editing